S2TD-Face: Reconstruct a Detailed 3D Face with Controllable Texture from a Single Sketch

Anonymous Authors

ABSTRACT

3D textured face reconstruction from sketches applicable in many scenarios such as animation, 3D avatars, artistic design, missing people search, *etc.*, is a highly promising but underdeveloped research topic. On the one hand, the stylistic diversity of sketches leads to existing sketch-to-3D-face methods only being able to handle pose-limited and realistically shaded sketches. On the other hand, texture plays a vital role in representing facial appearance, yet sketches lack this information, necessitating additional texture control in the reconstruction process. This paper proposes a novel method for reconstructing controllable textured and detailed 3D faces from sketches, named S2TD-Face. S2TD-Face introduces a two-stage geometry reconstruction framework that directly reconstructs detailed geometry from the input sketch. To keep geometry consistent with the delicate strokes of the sketch, we propose a novel sketch-to-geometry loss that ensures the reconstruction accurately fits the input features like dimples and wrinkles. Our training strategies do not rely on hard-to-obtain 3D face scanning data or labor-intensive hand-drawn sketches. Furthermore, S2TD-Face introduces a texture control module utilizing text prompts to select the most suitable textures from a library and seamlessly integrate them into the geometry, resulting in a 3D detailed face with controllable texture. S2TD-Face surpasses existing state-of-the-art methods in extensive quantitative and qualitative experiments. The code will be publicly available.

CCS CONCEPTS

• **Computing methodologies** → **Reconstruction**.

KEYWORDS

3D Face Reconstruction, Face Sketch, Rendering

1 INTRODUCTION

Reconstructing 3D textured faces from sketches has been a valuable research topic, finding applications in custom-made 3D avatars, artistic design, criminal investigation, *etc.* However, existing sketch-to-3D-face methods [28, 61] suffer from the following issues. On the one hand, the diverse styles of face sketches, ranging from realistic representations with detailed shading to cartoon-like drawings with simplified lines [60], pose challenges for existing methods that typically focus on sketches with frontal poses [28] or rely heavily on realistically shaded sketches as input [61]. On the other hand, texture plays a crucial role in accurately portraying facial appearance, highlighting the necessity for texture control within the sketch-to-3D-face process, while existing methods lack this capability. Furthermore, the absence of matching data between sketches and 3D faces makes it hard to train the framework. This paper proposes a method to reconstruct topology-consistent 3D faces with fine-grained geometry that precisely matches the input sketch and allows users to control the texture of reconstruction through text prompts, named **S2TD-Face** (**S**ketch to controllable **T**extured and **D**etailed **T**hree-**D**imensional **Face**). We introduce S2TD-Face in three parts: geometry reconstruction, training strategies, and texture control module.

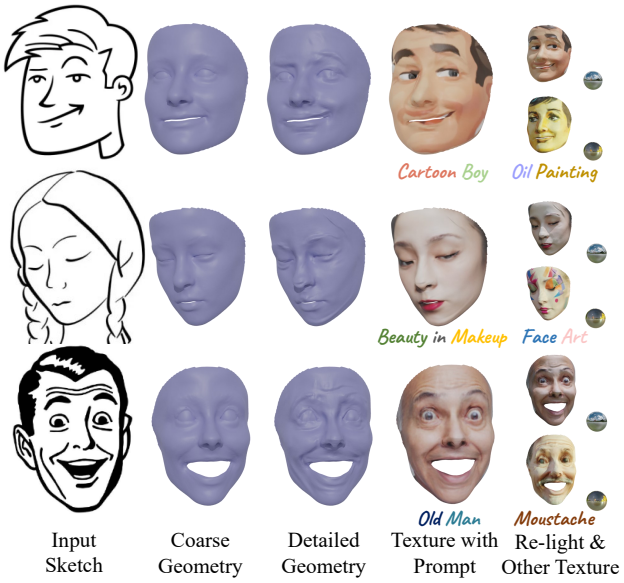

Figure 1: S2TD-Face can reconstruct high-fidelity geometry from face sketches. The texture control module seamlessly applies suitable textures onto the geometry based on prompts. The results can be re-lighted for various application scenes.

One straightforward approach to reconstructing 3D faces from sketches might involve first translating 2D sketches to 2D face images [13, 40, 52], followed by utilizing existing 3D face reconstruction methods [17, 19, 26, 31, 59, 66, 67] to obtain the 3D faces. However, this approach suffers from the following shortcoming. It heavily relies on the cooperation of both the sketch-to-image and image-to-3D-face stages, where inherently sparse but important geometric information like dimples or wrinkles in sketches is often lost during the transformation process, as the two transformation steps are independent, leaving sketches unable to directly constrain the final 3D geometry. In contrast, S2TD-Face uses a direct and efficient geometry reconstruction framework. It firstly predicts the coefficients of 3DMMs [4, 5] from input sketches to reconstruct

Unpublished working draft. Not for distribution.

ACM MM, 2024, Melbourne, Australia

ACM ISBN 978-x-xxxx-xxxx-x/YY/MM
https://doi.org/10.1145/nnnnnnn.nnnnnnn

coarse geometry and then utilizes coarse geometry and sketches in UV space to generate displacement maps for detailed geometry.

To ensure the framework reconstructs 3D detailed faces that accurately reflect the delicate features of the input, we introduce a novel sketch-to-geometry loss function to supervise both coarse and detailed geometry. This function combines differentiable rendering techniques [34, 51] to extract sketches of different styles from both geometry stages and compare them with ground truth sketches, guiding geometry deformation, as shown in Fig. 4. To ensure the robustness of the reconstruction framework across different sketch styles, we generate 5 different types of sketches for each face image by using traditional filtering operators [6] and deep learning methods [56, 57], as shown in Fig. 2 (a)-(e), with each sample randomly selecting a sketch type as input during training. The framework is trained by 2D signals like landmarks, segmentation, and perception features, as shown in Fig. 2 (f)-(h), without relying on the 3D face scanning data. Based on the widely-used REALY benchmark [9], we tailor it to better suit sketch-to-3D-face tasks for geometry evaluation by transforming the test samples into different styles of sketches, conducting fair evaluation on state-of-the-art methods [17, 19, 20, 26, 28, 37, 54]. Extensive experiments indicate that our method significantly outperforms existing methods.

S2TD-Face controls the texture of reconstructed 3D faces based on a text-image module, offering the following capabilities: it can search for suitable texture from a face library based on the text prompt, transform the selected texture information to UV space, and seamlessly apply the UV-texture to the reconstructed geometry. As shown in the first row of Fig. 1, when the user provides a text prompt describing the desired texture, S2TD-Face can reconstruct 3D textured faces in styles such as *'Cartoon Boy'* or *'Oil Painting'*.

In summary, the main contributions of S2TD-Face are as follows:

- An effective framework for reconstructing 3D detailed high-fidelity faces from sketches with a novel sketch-to-geometry loss, which accurately captures the local strokes of the input.
- A novel texture control module for controlling the texture of the reconstructions, resulting in textured 3D faces with various styles ranging from cartoons to realistic appearances.
- Extensive experiments show that our method achieves excellent performance and outperforms the existing methods.

2 RELATED WORK

3D Face Reconstruction. Reconstructing 3D faces from 2D images has achieved widespread success. Methods such as [17, 19, 26, 37, 59, 66, 67] can generate realistic 3D faces from facial images captured in various poses, environments, and expressions. These methods typically utilize 2D landmarks, segmentation, texture information, *etc.* to guide the deformation of 3DMMs [4, 5], and further leverage differentiable rendering techniques [14, 21, 34, 41, 51, 55] for fine-grained reconstruction [19, 37]. These validated 2D-to-3D supervision approaches are applicable for training sketch-to-3D-face framework. Some methods [2, 18, 24, 35, 36] focus on texture reconstruction. They typically decompose textures into components such as diffuse, specular, ambient occlusion, normal, and translucency, applicable in re-rendering in new environments or creating 3D avatars. However, the textures provided by these methods lack diversity, missing complex styles such as cartoon styles or makeup as shown in Fig. 1, and still exhibit disparities in high-frequency details compared to textures directly derived from image UV mapping.

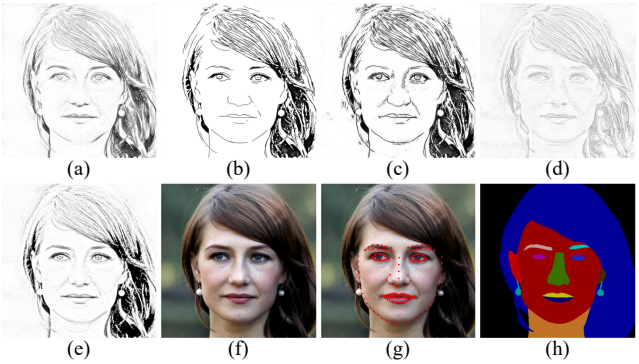

Figure 2: Data samples of S2TD-Face. (a)-(e) are sketches in different styles generated from the original image (f). (g) represents landmarks, and (h) represents segmentation. Inputs of the pipeline include sketches (a)-(e) and (f)-(h) serve as supervisory signals.

Translate Sketches to Other Modalities. Some methods [3, 22, 25, 43, 62, 64] reconstruct 3D shapes from sketches of common objects such as cups, chairs, cars, airplanes, *etc.* They typically supervise the 3D geometry based on 2D silhouettes using differential renderers [62], involving point set matching and optimization (such as chamfer distance) [22, 25], or innovation in 3D representation forms (such as Signed Distance Fields [46]) [43, 64]. These methods are usually limited to specific types of objects, and a domain gap exists when reconstructing faces. Few methods reconstruct 3D faces from facial sketches, they either specialize in sketches with frontal poses [28] or heavily depend on professional sketches with precise shading as input [61], which may not align with practical requirements. Some methods [11–13, 23, 40, 52] translate facial sketches into 2D face images, often utilizing frameworks such as Generative Adversarial Networks (GANs) [15] or Neural Radiance Fields (NeRFs) [45] to synthesize face images. Combining these sketch-to-face-image methods with image-to-3D-face methods [19, 59, 66] seems like a straightforward solution. However, the local stroke information of the original input sketch (such as dimples, wrinkles, *etc.*) is easily lost in this process, leading to reconstruction results that are not consistent with the input sketches.

3 METHODOLOGY

3.1 Preliminaries

Data Processing. For a given RGB face image $\boldsymbol{I} \in \mathbb{R}^{H\times W\times 3}$, based on the common practices in [13, 52, 56, 57], we generate 5 types of sketches $\boldsymbol{S}_{t_i} \in \mathbb{R}^{H\times W\times 3}$:

$$\boldsymbol{S}_{t_i} = \boldsymbol{\Phi}_{\text{sketch}}(\boldsymbol{I}, t_i) \ , \tag{1}$$

where we integrate existing various sketch operations [7, 56, 57] into a single function $\boldsymbol{\Phi}_{\text{sketch}}(\cdot)$. We make $\boldsymbol{\Phi}_{\text{sketch}}(\cdot)$ differentiable and will also apply it to the sketch-to-geometry loss. t_i represents different sketch types, $i \in [1, \cdots, 5]$, as illustrated in Fig. 2(a)-(e). Following [59], we utilize landmark detectors [59] to obtain 2D landmarks $\boldsymbol{lmk} \in \mathbb{R}^{2\times 240}$ and employ DML-CSR [63] to generate

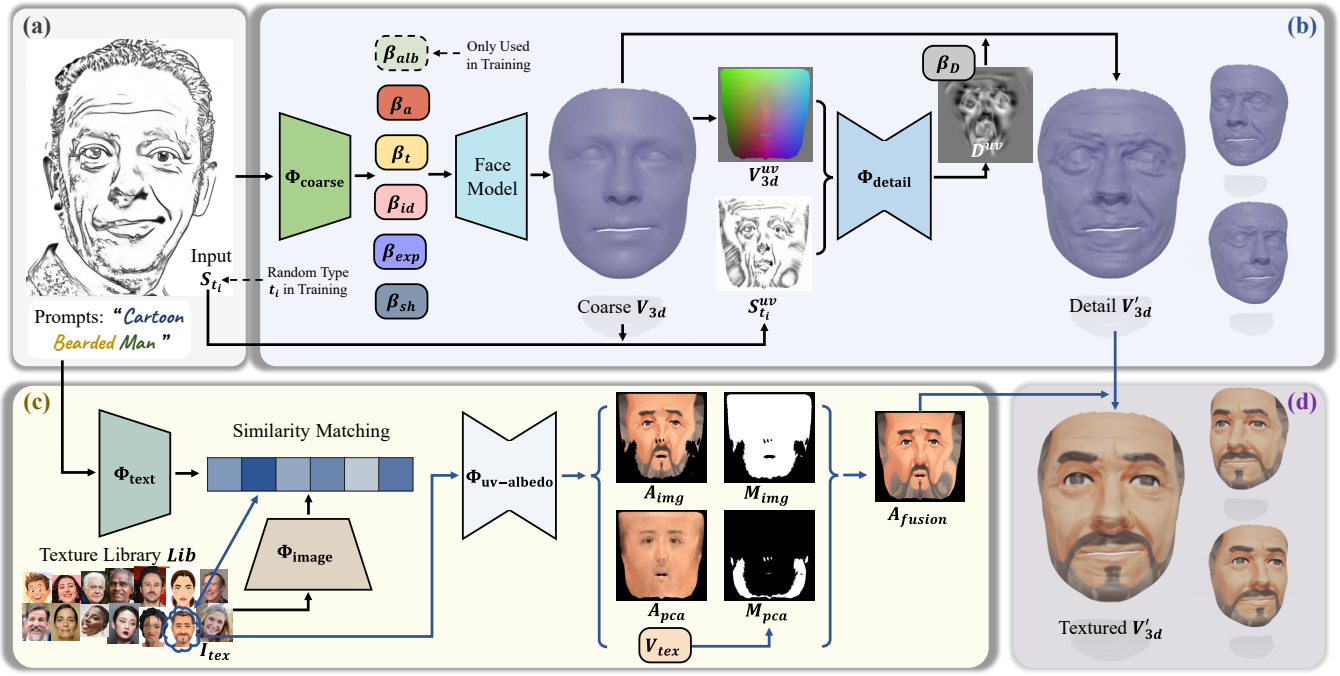

Figure 3: Overview of our method. (a) The input of S2TD-Face: a face sketch and a text prompt. (b): The geometry reconstruction framework yields detailed 3D faces that accurately reflects the delicate features of the input sketches. (c): The texture control module seamlessly applies the controllable texture to the geometry with text prompts. (d) The output of S2TD-Face: a detailed 3D face with controllable texture.

segmentation information C for supervisory signals in geometry. These data processing methods enable S2TD-Face to acquire training data from existing abundant face datasets [32, 38, 39, 42, 44, 53], without relying on hard-to-collect 3D face scanning data or labor-intensive hand-drawn sketches. In summary, during the training process, each data sample consists of sketches $\{S_{t_i}\}$, original face image I, segmentation C, and landmarks lmk, as shown in Fig. 2.

Face Model. Based on [8, 27, 48], we define the coarse vertices and albedo of a 3D face using the following formula:

$$\begin{aligned} V_{3d} &= R(\beta_a)(\overline{V} + \beta_{id}B_{id} + \beta_{exp}B_{exp}) + \beta_t \\ T_{alb} &= \overline{T} + \beta_{alb}B_{alb} \end{aligned} , \tag{2}$$

where $\overline{V}$ and $\overline{T}$ are the mean geometry and the mean albedo, respectively. $V_{3d} \in \mathbb{R}^{3\times 35709}$ is the coarse face vertices and $T_{alb} \in \mathbb{R}^{3\times 35709}$ is the albedo. $\beta_{id} \in \mathbb{R}^{80}$, $\beta_{exp} \in \mathbb{R}^{64}$ and $\beta_{alb} \in \mathbb{R}^{80}$ are the identity geometry parameter, the expression geometry parameter and the albedo parameter, respectively. B_{id}, B_{exp} and B_{alb} are the face identity bases, the expression bases and the albedo bases, respectively. We utilize angles $\beta_a \in \mathbb{R}^3$ (pitch, yaw, and roll) to obtain the rotation matrix $R(\beta_a) \in \mathbb{R}^{3\times 3}$, for the rotation of V_{3d}. We employ $\beta_t \in \mathbb{R}^3$ to control the translation of V_{3d}. Note that T_{alb} is not the final facial texture and it will not appear during the inference process of the framework. T_{alb} solely assists in supervising the geometry during the training process.

Face Attributes in UV Space. UV mapping is a reversible 3D modeling process commonly used to project the attributes of 3D objects into the 2D image plane. We can transfer facial geometry information, facial texture information, and other attributes to UV space. These techniques are employed in many 3D face reconstruction methods [10, 18, 20], often combined with differentiable renderers [34, 51], facial texture completion [2, 10, 18], and illumination estimation [19]. In the following section, we denote the facial attribute X in UV space as X^{uv}.

Camera. Following [17, 37, 59], we utilize a camera with a fixed perspective projection for the re-projection of V_{3d} into the 2D image plane, yielding $V_{2d} \in \mathbb{R}^{2\times 35709}$.

Illumination Model. Based on [17, 19], we employ Spherical Harmonics (SH) [50] to predict the shading information:

$$S(\beta_{sh}, A, N) = A \odot \sum_{k=1}^{9} \beta_{sh}^k \Psi_k(N) , \tag{3}$$

where $\odot$ denotes the Hadamard product, N is the surface normal of V_{3d}, $\Psi : \mathbb{R}^3 \rightarrow \mathbb{R}$ is the SH basis function and $\beta_{sh}^k \in \mathbb{R}^3$ is the corresponding SH parameter, $k \in [1, \cdots, 9]$. A represents the albedo information, which could be set as T_{alb} to calculate the shaded texture. Following [19, 37], we also set A to a fixed gray value A_{gray} to display the geometry shading.

Detail Reconstruction. The coarse geometry V_{3d} based on 3DMMs can not capture the high-frequency details of a 3D face. To address this, we perform detail reconstruction based on [19, 37], which is achieved by computing a displacement map:

$$V'_{3d}{}^{uv} = V_{3d}{}^{uv} + \beta_D D^{uv} \odot N^{uv} , \tag{4}$$

where $D^{uv} \in \mathbb{R}^{256\times 256}$ represents the detail displacement map in UV space. $V_{3d}{}^{uv} \in \mathbb{R}^{256\times 256\times 3}$ and $V'_{3d}{}^{uv} \in \mathbb{R}^{256\times 256\times 3}$ denote

the coarse geometry and detail geometry in UV space, respectively. $\boldsymbol{N}^{uv} \in \mathbb{R}^{256\times256\times3}$ represents the surface normal corresponding to ${V_{3d}}^{uv}$. $\boldsymbol{\beta}_D \in \mathbb{R}^+$ is used to control the magnitude of the displacement map $\boldsymbol{D}^{uv}$. We denote the surface normal of the detail geometry ${V'}_{3d}$ as $\boldsymbol{N'}$.

Rendering. Based on [19, 34, 51], we construct a differentiable renderer $\Phi_{\text{render}}(\cdot)$ using the fixed camera, which could yield the following results:

$$\begin{aligned} \boldsymbol{I}^a &= \Phi_{\text{render}}(V_{3d}, S(\boldsymbol{\beta}_{sh}, T_{alb}, \boldsymbol{N})) \\ \boldsymbol{I}^b &= \Phi_{\text{render}}(V_{3d}, S(\boldsymbol{\beta}_{sh}, T_{alb}, \boldsymbol{N'})) \\ \boldsymbol{I}^c &= \Phi_{\text{render}}(V_{3d}, S(\boldsymbol{\beta}_{sh}, \boldsymbol{A}_{gray}, \boldsymbol{N})) \\ \boldsymbol{I}^d &= \Phi_{\text{render}}(V_{3d}, S(\boldsymbol{\beta}_{sh}, \boldsymbol{A}_{gray}, \boldsymbol{N'})) \end{aligned} , \tag{5}$$

where the input of the differentiable renderer $\Phi_{\text{render}}(\cdot)$ includes coarse geometry and shading information, achieving detailed rendering effects through the refinement of the normal map in the shading information. The rendering results $\boldsymbol{I}^a$, $\boldsymbol{I}^b$, $\boldsymbol{I}^c$, and $\boldsymbol{I}^d$ represent the coarse texture, detail texture, coarse geometry shading, and detail geometry shading, respectively, which are used in sketch-to-geometry loss, as shown in Fig. 4.

3.2 Geometry Reconstruction Framework

We aim to reconstruct detailed geometry consistent with the delicate features of the input sketch. The sketch-to-3D-face process of S2TD-Face is divided into two stages: coarse geometry reconstruction and detailed geometry reconstruction, as shown in Fig. 3(b).

Coarse Geometry Reconstruction. During the training process, for each data sample, we randomly select a sketch $\boldsymbol{S}_{t_i}$ of type t_i as input. We employ ResNet-50 [29] as the backbone Φ_{coarse} to predict parameters $\boldsymbol{\beta}_a$, $\boldsymbol{\beta}_t$, $\boldsymbol{\beta}_{id}$, $\boldsymbol{\beta}_{exp}$, $\boldsymbol{\beta}_{sh}$, and $\boldsymbol{\beta}_{alb}$. These parameters are processed by the face model [8, 48] to generate coarse geometry V_{3d} and the PCA albedo T_{alb}, as described in Eqn. 2. T_{alb} is used for photometric loss $\mathcal{L}_{\text{pho}}$, perception loss $\mathcal{L}_{\text{per}}$, and sketch-to-geometry loss $\mathcal{L}_{\text{sketch}}$. Note that during the inference, there are no restrictions on the sketch types, and neither T_{alb} nor $\boldsymbol{\beta}_{alb}$ are involved. Additionally, $\boldsymbol{\beta}_{sh}$ for controlling light can vary as shown in Fig. 1. We utilize V_{3d} to map the sketch image $\boldsymbol{S}_{t_i}$ to UV space, resulting in $\boldsymbol{S}_{t_i}^{uv}$. $\boldsymbol{S}_{t_i}^{uv}$. The UV space representation V_{3d}^{uv} of V_{3d} will jointly serve as the input for reconstructing the detailed geometry.

Detailed Geometry Reconstruction. Using V_{3d}^{uv} and $\boldsymbol{S}_{t_i}^{uv}$ as input, we employ a pix2pix network [30] Φ_{detail} to predict the displacement map $\boldsymbol{D}^{uv}$ for reconstructing the detailed geometry ${V'}_{3d}{}^{uv}$ in Eqn. 4. Throughout this process, $\boldsymbol{\beta}_D$ serves as a learnable parameter controlling the magnitude of $\boldsymbol{D}^{uv}$, which is fixed during inference.

3.3 Training Strategies

To train Φ_{coarse} and Φ_{detail} in S2TD-Face, we employ the following training methods and supervision loss functions.

Various Sketch Types. The facial sketch types are diverse, with some containing realistic shading information, while others only consist of simple lines. To ensure the robustness of Φ_{coarse} and Φ_{detail} across different sketches, randomization is applied to all operations involving sketch type selection during the training process. Specifically, the training input employs a random sketch type t_i, as shown in Fig. 3(b), and in the sketch-to-geometry loss $\mathcal{L}_{\text{sketch}}$, the type t_j is also randomly selected, as shown in Fig. 4. These strategies ensures that Φ_{coarse} and Φ_{detail} possess strong adaptability to different sketch types.

Sketch-to-geometry Loss. Existing supervision methods fail to accurately capture the local details of sketches (such as dimples, wrinkles, *etc.*) and reflect them onto the geometry deformation. To address this, we propose a novel sketch-to-geometry loss $\mathcal{L}_{\text{sketch}}$ to ensure the geometry V_{3d} and ${V'}_{3d}$ fidelity to the sketch input and supervise Φ_{coarse} and Φ_{detail} robustly across different sketch types, as shown in Fig. 4. Based on the rendering results $\boldsymbol{I}^a$, $\boldsymbol{I}^b$, $\boldsymbol{I}^c$, and $\boldsymbol{I}^d$, we further utilize $\Phi_{\text{sketch}}(\cdot)$ to generate the corresponding sketches $\boldsymbol{S}_{t_j}^a$, $\boldsymbol{S}_{t_j}^b$, $\boldsymbol{S}_{t_j}^c$, and $\boldsymbol{S}_{t_j}^d$:

$$\boldsymbol{S}_{t_j}^n = \Phi_{\text{sketch}}(\boldsymbol{I}^n, t_j), \text{for } n \in \{a, b, c, d\} \ , \tag{6}$$

where type t_j is randomly selected. Since Φ_{coarse}, Φ_{detail}, Φ_{render}, and Φ_{sketch} are all differentiable, and we have the sketch ground truth $\boldsymbol{S}_{t_j}$ corresponding to the type t_j, we could compare the differences between $\left\{\boldsymbol{S}_{t_j}^n \middle| n \in \{a, b, c, d\}\right\}$ and $\boldsymbol{S}_{t_j}$ by using photometric loss and perception loss:

$$\begin{aligned} \mathcal{L}_{\text{sketch}} = \lambda_1 \underbrace{\sum_{n\in\{a,b,c,d\}} \left\|\boldsymbol{M}^n - \boldsymbol{M}\right\|_2}_{\text{sketch-photometric}} \\ + \lambda_2 \underbrace{\sum_{n\in\{a,b,c,d\}} \left(1 - \frac{< \Phi_{\text{per}}(\boldsymbol{M}^n), \Phi_{\text{per}}(\boldsymbol{M}) >}{||\Phi_{\text{per}}(\boldsymbol{M}^n)||_2 \cdot ||\Phi_{\text{per}}(\boldsymbol{M})||_2}\right)}_{\text{sketch-perception}} \end{aligned} , \tag{7}$$

where $\mathcal{L}_{\text{sketch}}$ contains two error parts: photometric error and perception error. The former computes L2-norm error, while the latter computes the cosine distance. λ_1 and λ_2 are the corresponding weights. $\Phi_{\text{per}}(\cdot)$ is a face recognition network from [17], used to extract features from the input, and $< \cdot, \cdot >$ denotes the vector inner product. $\boldsymbol{M}^n$ and $\boldsymbol{M}$ respectively represent the mask-filtered results of $\left\{\boldsymbol{S}_{t_j}^n \middle| n \in \{a, b, c, d\}\right\}$ and $\boldsymbol{S}_{t_j}$, *i.e.* $\boldsymbol{M}^n = \boldsymbol{M}_C \odot \boldsymbol{M}_{render} \odot \boldsymbol{S}_{t_j}^n$, for $n \in \{a, b, c, d\}$ and $\boldsymbol{M} = \boldsymbol{M}_C \odot \boldsymbol{M}_{render} \odot \boldsymbol{S}_{t_j}$. $\boldsymbol{M}_C$ and $\boldsymbol{M}_{render}$ respectively represent the masks obtained by segmentation information $\boldsymbol{C}$ and Φ_{render}, as shown in Fig. 4. Combining with the mask-filtered results can eliminate interference caused by occlusions and focus on the rendering object.

Photometric Loss and Perception Loss for $\boldsymbol{I}^b$. To enhance the robustness of the training process, we supervise the detail texture rendering result $\boldsymbol{I}^b$ in Eqn. 5 similar to [19, 37]. Note that this process operates at the rendering image level $\boldsymbol{I}^b$, while $\mathcal{L}_{\text{sketch}}$ operates at the rendering sketch level. The photometric loss $\mathcal{L}_{\text{pho}}$ and perception loss $\mathcal{L}_{\text{per}}$ used are defined as follows:

$$\mathcal{L}_{\text{pho}} = \left\|(\boldsymbol{MI}^b - \boldsymbol{MI})\right\|_2 \ , \tag{8}$$

$$\mathcal{L}_{\text{per}} = 1 - \frac{< \Phi_{\text{per}}(\boldsymbol{MI}^b), \Phi_{\text{per}}(\boldsymbol{MI}) >}{\left\|\Phi_{\text{per}}(\boldsymbol{MI}^b)\right\|_2 \cdot \left\|\Phi_{\text{per}}(\boldsymbol{MI})\right\|_2}, \tag{9}$$

where $\boldsymbol{MI}^b = \boldsymbol{M}_C \odot \boldsymbol{M}_{render} \odot \boldsymbol{I}^b$ and $\boldsymbol{MI} = \boldsymbol{M}_C \odot \boldsymbol{M}_{render} \odot \boldsymbol{I}$. Similar to the operations in $\mathcal{L}_{\text{sketch}}$, $\Phi_{\text{per}}(\cdot)$ is a face recognition network [17] and $< \cdot, \cdot >$ is the vector inner product. We emphasize

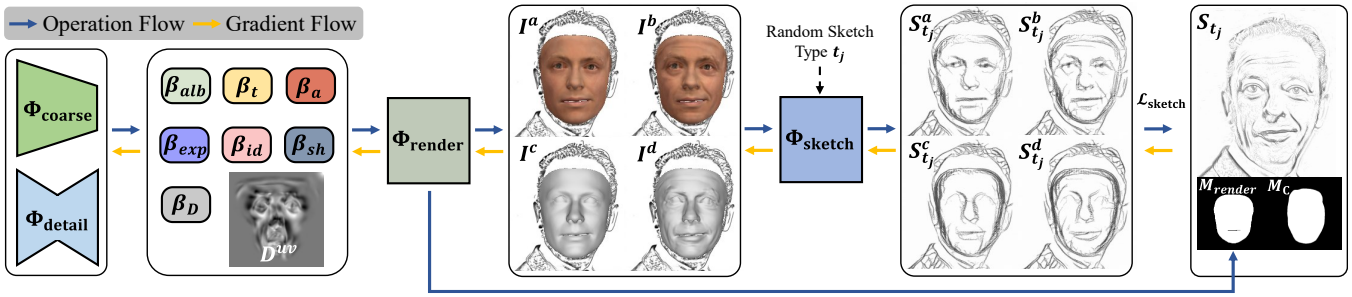

Figure 4: Overview of sketch-to-geometry loss. $\mathcal{L}_{\text{sketch}}$ compares the predicted sketches $\{S^a_{t_j}, S^b_{t_j}, S^c_{t_j}, S^d_{t_j}\}$ with the ground truth S_{t_j} to supervise the geometry deformation, obtaining detailed geometry consistent with the delicate features of the input.

again that in $\mathcal{L}_{\text{sketch}}$, $\mathcal{L}_{\text{pho}}$, and $\mathcal{L}_{\text{per}}$, the texture of I^a or I^b is derived from T_{alb}, aims to supervise the geometry. T_{alb} is not the final texture and will not appear in the inference process.

Landmark Loss. We employ landmark loss to compare the predicted 2D landmarks $\boldsymbol{lmk}'$ from V_{2d} with the ground truth $\boldsymbol{lmk}$ obtained by [59], adopting the dynamic landmark marching [65] to address the non-correspondence between 2D and 3D cheek contour caused by pose variations. The landmark loss $\mathcal{L}_{\text{lmk}}$ is defined as:

$$\mathcal{L}_{\text{lmk}} = \sum_{i=1}^{240} \left\| \boldsymbol{lmk}'_i - \boldsymbol{lmk}_i \right\|_2. \tag{10}$$

Part Re-projection Distance Loss. Since $\mathcal{L}_{\text{lmk}}$ can only operate on sparse vertices in V_{2d}, we further utilize Part Re-projection Distance Loss (PRDL) [59] $\mathcal{L}_{\text{prdl}}$ to supervise V_{2d}. $\mathcal{L}_{\text{prdl}}$ leverages the precise 2D part silhouettes provided by segmentation C to constrain the predicted geometry of facial features:

$$\mathcal{L}_{\text{prdl}} = \sum_{p \in P} \lambda_p \left\| \mathbf{\Gamma}_p(V_{2d}) - \mathbf{\Gamma}_p(C) \right\|_2, \tag{11}$$

where P represents the set of facial components, P = {left_eye, right_eye, left_eyebrow, right_eyebrow, up_lip, down_lip, nose, skin}. $\mathbf{\Gamma}_p(V_{2d})$ and $\mathbf{\Gamma}_p(C)$ respectively denote the shape descriptors of PRDL defined for prediction and target in [59]. λ_p represents the weight of each part p. During training, specific parts p of samples may be occluded or invisible, we set $\lambda_p = 0$ for parts p in these samples and $\lambda_p = 1$ for the rest parts.

Overall Losses. In summary, we minimize the total loss $\mathcal{L}$ to optimize the geometry reconstruction frameworks Φ_{coarse} and Φ_{detail}:

$$\begin{aligned} \mathcal{L} = {} & \lambda_{\text{sketch}}\mathcal{L}_{\text{sketch}} + \lambda_{\text{pho}}\mathcal{L}_{\text{pho}} + \lambda_{\text{per}}\mathcal{L}_{\text{per}} \\ & + \lambda_{\text{lmk}}\mathcal{L}_{\text{lmk}} + \lambda_{\text{prdl}}\mathcal{L}_{\text{prdl}} + \lambda_{\text{reg}}\mathcal{L}_{\text{reg}}, \end{aligned} \tag{12}$$

where $\mathcal{L}_{\text{reg}}$ is the regularization loss for parameters $\boldsymbol{\beta}$. $\lambda_{\text{sketch}} = 1$, $\lambda_1 = 1.33$, $\lambda_2 = 0.1$, $\lambda_{\text{pho}} = 0.57$, $\lambda_{\text{per}} = 0.1$, $\lambda_{\text{lmk}} = 1.6e-3$, $\lambda_{\text{prdl}} = 8e-4$, and $\lambda_{reg} = 3e-4$ are the corresponding weights. $\mathcal{L}_{\text{lmk}}$ and $\mathcal{L}_{\text{prdl}}$ are normalized by $H \times W$.

Training Details. We firstly train Φ_{coarse}, then freeze Φ_{coarse} to train Φ_{detail} and finally train Φ_{coarse} and Φ_{detail} together. Therefore, during the first training stage when using $\mathcal{L}_{\text{sketch}}$, $S^b_{t_j}$ and $S^d_{t_j}$ are not used, and I^b in $\mathcal{L}_{\text{pho}}$ and $\mathcal{L}_{\text{per}}$ is replaced by I^a.

3.4 Texture Control Module

We aim to design a texture control module for S2TD-Face that can select appropriate samples from a given texture library based on input text prompts, obtain textures in UV space, and seamlessly map them onto the geometry V'_{3d}. As illustrated in the Fig. 3(c), when the input prompt $Text$ is *'Cartoon Beard Man'*, we use Φ_{image} and Φ_{text} from CLIP [49] to encode the face images I^i_{Lib} from the known texture library Lib and the input text $Text$:

$$\begin{aligned} F^I_i &= \Phi_{\text{image}}(I^i_{Lib}),\ i = 1, 2, \cdots, |Lib| \\ F^T &= \Phi_{\text{text}}(Text) \end{aligned}, \tag{13}$$

where F^I_i and F^T are the image encoding features and the text encoding features, respectively. $|Lib|$ is the image number in the given texture library Lib. In the text-to-image matching process, each F^I_i is compared to F^T to compute similarity, and S2TD-Face can either select the image with maximum similarity to the input text or randomly choose one from the top-k similar images. We denote the final matching result as I_{tex}.

The role of $\Phi_{\text{uv-albedo}}$ in the texture control module is to transform the texture of the face image into UV spcae that are compatible with V'_{3d}. We input the text-image matching result I_{tex} to $\Phi_{\text{uv-albedo}}$ to get the desired texture information in UV space. Specifically, $\Phi_{\text{uv-albedo}}$ is based on the state-of-the-art monocular 3D face reconstruction method [59]. $\Phi_{\text{uv-albedo}}$ firstly estimates the 3DMMs [8, 48] shape V_{tex} and the PCA albedo A_{pca} from I_{tex}, and then utilizes the shape information V_{tex} to map the input image I_{tex} into UV space, obtaining A_{img}, as shown in the Fig. 3(c). Due to the pose influence of V_{tex}, some facial areas of I_{tex} are invisible and the UV-texture information A_{img} may not cover the entire facial surface. Therefore, $\Phi_{\text{uv-albedo}}$ calculates the invisible areas according to V_{tex} and complete UV-texture using A_{pca}, finally resulting in the fusion texture A_{fusion}:

$$A_{fusion} = M_{img} \odot A_{img} + M_{pca} \odot A_{pca}, \tag{14}$$

where M_{img} is a mask computed by the differentiable renderer Φ_{render} with the help of V_{tex}, which represents the visible regions of the reconstructed shape V_{tex} that consistent with the input texture mapping A_{img}. $M_{pca} = 1 - M_{img}$ indicates the regions that require further complement by the predicted 3DMMs PCA albedo A_{pca}. To reduce visual differences at the fusion boundaries, we apply median filtering [7] to M_{img}. The texture control module finally applies A_{fusion} onto the geometry V'_{3d} through UV mapping, resulting in a detailed and textured 3D face, as shown in the Fig. 3(d).

Table 1: Quantitative comparison on Sketch-REALY benchmark. We transform the test samples from REALY [9] into two types of sketches: 'Shading' (realistic shaded sketches) and 'Line' (sparse line sketches), as shown in Fig. 5, and perform quantitative comparison respectively. Lower values indicate better results. The best and runner-up are highlighted in bold and underlined, respectively. We also investigate the effect of removing the sketch-to-geometry loss $\mathcal{L}_{\text{sketch}}$ (denoted as 'Ours (w/o $\mathcal{L}_{\text{sketch}}$)') for ablation study.

Types	Methods	*Frontal-view (mm)* ↓					*Side-view (mm)* ↓				
		Nose avg.± std.	*Mouth* avg.± std.	*Forehead* avg.± std.	*Cheek* avg.± std.	*avg.*	*Nose* avg.± std.	*Mouth* avg.± std.	*Forehead* avg.± std.	*Cheek* avg.± std.	*avg.*
Shading	PRNet [20]†	2.047±0.498	1.750±0.569	2.400±0.586	1.896±0.694	2.023	2.027±0.507	1.880±0.591	2.525±0.643	2.093±0.757	2.131
	MGCNet [54]†	1.711±0.422	1.617±0.552	2.194±0.567	1.609±0.588	1.783	1.685±0.438	1.555±0.511	2.189±0.560	1.656±0.597	1.771
	Deep3D[17]†	1.781±0.430	1.714±0.592	2.124±0.482	1.274±0.461	1.723	1.658±0.350	1.830±0.663	2.147±0.502	1.284±0.466	1.730
	3DDFA-V2 [26]†	1.866±0.498	1.722±0.503	2.509±0.687	1.956±0.709	2.013	1.856±0.489	1.724±0.522	2.535±0.660	1.993±0.723	2.027
	HRN [37]†	1.723±0.435	1.878±0.623	2.202±0.497	1.246±0.424	1.762	1.647±0.369	1.957±0.693	2.245±0.515	1.269±0.420	1.779
	DECA [19]†	1.830±0.405	2.475±0.793	2.420±0.598	1.600±0.597	2.081	1.858±0.428	2.542±0.836	2.448±0.610	1.628±0.607	2.119
	DeepSketch2Face [28]	3.896±0.774	2.808±1.392	5.091±0.899	6.450±0.972	4.561	3.950±0.810	3.250±1.669	5.489±1.069	6.746±1.038	4.859
	Ours (w/o $\mathcal{L}_{\text{sketch}}$)	**1.621±0.323**	1.454±0.487	2.021±0.492	1.288±0.378	1.596	1.594±0.317	1.482±0.509	2.041±0.565	1.299±0.385	1.604
	Ours	1.630±0.348	**1.324±0.412**	**1.986±0.418**	**1.191±0.343**	**1.533**	**1.559±0.329**	**1.357±0.469**	**1.960±0.471**	**1.149±0.336**	**1.506**
Line	PRNet [20]†	2.166±0.553	2.127±0.648	2.714±0.787	2.164±0.798	2.293	2.138±0.552	2.243±0.821	3.071±0.985	2.422±0.894	2.468
	MGCNet [54]†	2.114±0.632	2.257±0.851	2.881±0.946	1.714±0.630	2.241	2.039±0.532	2.019±0.730	2.840±0.994	1.800±0.689	2.175
	Deep3D[17]†	2.230±0.513	1.865±0.646	2.290±0.550	1.487±0.542	1.968	1.975±0.483	1.876±0.650	2.354±0.605	1.475±0.549	1.920
	3DDFA-V2 [26]†	1.965±0.561	2.045±0.685	2.632±0.798	1.931±0.752	2.143	1.968±0.551	2.056±0.672	2.681±0.838	1.976±0.805	2.170
	HRN [37]†	2.152±0.553	1.974±0.654	2.579±0.720	1.614±0.692	2.080	2.057±0.547	2.089±0.736	2.669±0.839	1.580±0.609	2.099
	DECA [19]†	2.121±0.490	2.598±0.914	2.703±0.606	1.641±0.573	2.266	2.071±0.482	2.559±0.947	2.757±0.696	1.630±0.573	2.254
	DeepSketch2Face [28]	3.359±0.653	2.483±0.595	4.835±0.994	5.464±1.074	4.035	3.726±0.895	2.701±0.717	5.150±1.037	6.124±1.086	4.425
	Ours (w/o $\mathcal{L}_{\text{sketch}}$)	**1.688±0.359**	1.755±0.640	2.288±0.553	1.477±0.383	1.802	1.675±0.352	1.798±0.594	2.316±0.618	1.495±0.397	1.821
	Ours	1.692±0.366	**1.524±0.505**	**2.131±0.510**	**1.344±0.385**	**1.673**	**1.627±0.350**	**1.556±0.476**	**2.227±0.570**	**1.352±0.377**	**1.690**

† There are two ways to reconstruct 3D faces from sketches based on existing SOTA methods [17, 19, 20, 26, 37, 54]: firstly translating 2D sketches to face images [52] and subsequently reconstructing 3D faces or directly using sketches as input. **For fairness, methods marked with † represent the best results obtained from these two ways.**

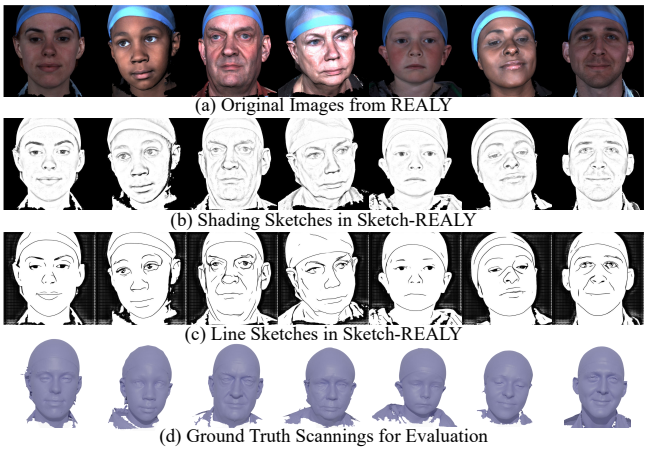

(a) Original Images from REALY

(b) Shading Sketches in Sketch-REALY

(c) Line Sketches in Sketch-REALY

(d) Ground Truth Scannings for Evaluation

Figure 5: The test samples (7/100) of Sketch-REALY. (a): The original test images from REALY [9]. (b) and (c): The 2 styles (Shading and Line) of the test images in Sketch-REALY. (d): The face scanning for geometry evaluation in Sketch-REALY.

4 EXPERIMENTS

4.1 Experimental Settings

Implementation Details. We implement S2TD-Face based on PyTorch [47]. The input sketches are resized into 224×224. $A_{gray} = (127, 127, 127)$. We use Adam [33] as the optimizer with an initial learning rate of $1e-4$. B_{id} and B_{alb} are from BFM2009 [48] and B_{exp} is from FaceWarehouse [8].

Data. We utilize face images from publicly available datasets, including CelebA [42], 300W [53], RAF [38, 39], and DAD-3DHeads [44], which are commonly used in 3D face reconstruction tasks. We employ [66] for face pose augmentation and [59] for face expression augmentation. As a result, we obtain about $600K$ face images for training. $\mathbf{\Phi}_{\text{sketch}}$ is based on [7, 56, 57] and each face image is processed by $\mathbf{\Phi}_{\text{sketch}}$ to obtain 5 different styles of sketches as input to the framework (resulting in $5 \times 600K$ sketches). The images in the texture library *Lib* of the texture control module are sourced from FFHQ [32] and online collections, totaling about 1000 images.

4.2 Metrics

Sketch-REALY. The REALY benchmark [9] comprises 100 precise 3D face scanning data (as shown in Fig. 5 (d)) from LYHM [16], which are from different identities and include accurate landmarks, region masks, and topology-consistent meshes. During the evaluation, REALY initially aligns the prediction and ground truth using landmarks. It subsequently divides the reconstructed results into 4 parts (nose, mouth, forehead, and cheek) using region masks. Finally, it utilizes the ICP algorithm [1] for precise registration between prediction and ground truth and computes the corresponding average Normalized Mean Square Error (NMSE) for different face regions. The REALY test samples are divided into 2 parts, consisting of 100 frontal-view images and 400 side-view images. REALY has served as the benchmark for geometric evaluation by most state-of-the-art methods [10, 18, 59]. We propose a new Sketch-REALY benchmark based on REALY [9] to tailor it for sketch-to-3D-face reconstruction tasks, highlighting the performance of geometry

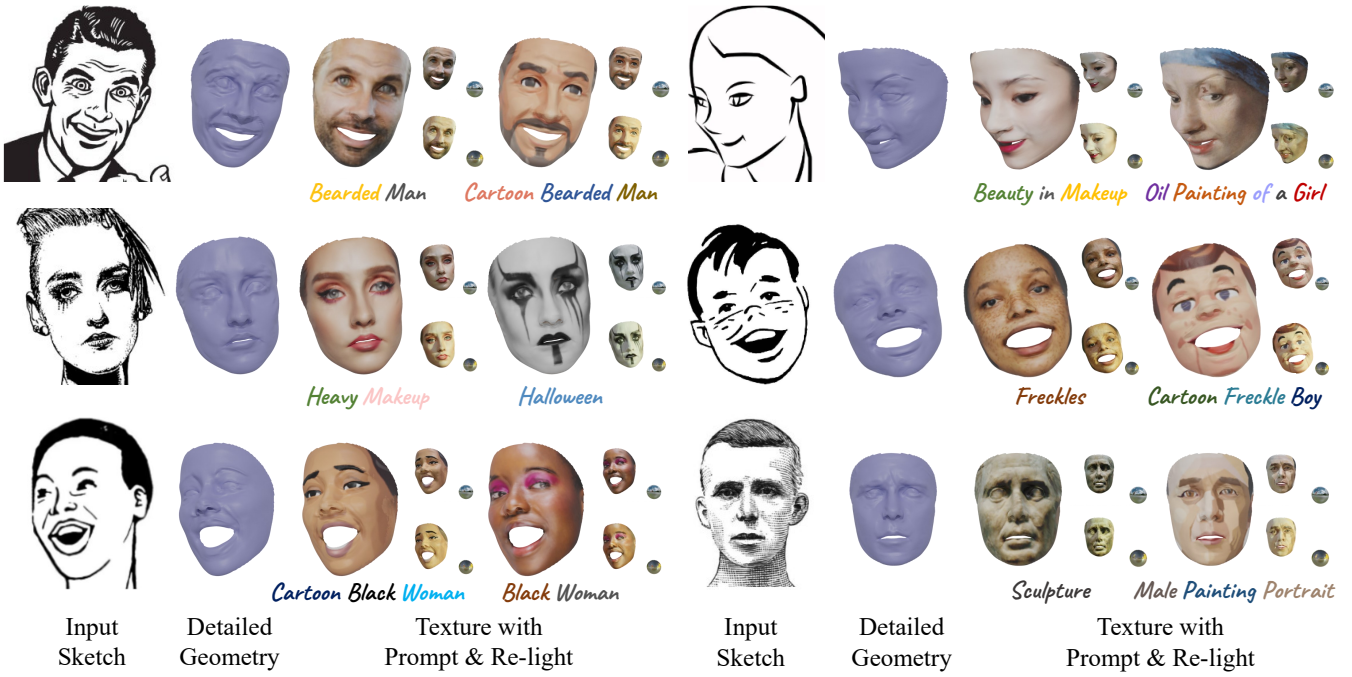

Figure 6: More visualization results of our method (S2TD-Face). S2TD-Face can reconstruct high-fidelity geometry from face sketches of different styles and generate controllable textures spanning cartoon, sculptural, and realistic facial styles guided by text prompts. The results can also be re-lighted for broader applications.

reconstruction from sketches. Specifically, we use Φ_{sketch} to process the REALY test images, generating 2 different types of sketches. The former retains the shading information from the original images, resembling realistic grayscale images (denoted as 'Shading'), while the latter only consists of sparse lines (denoted as 'Line'), as shown in Fig. 5 (b) and (c). We conduct the geometry evaluation on the 3D prediction of these two types of sketches, thereby establishing the Sketch-REALY benchmark.

SSIM and PSNR. Structural Similarity Index Measure (SSIM) [58] and Peak Signal to Noise Ratio (PSNR) are two standard metrics used to measure the similarity between images. SSIM considers the brightness, contrast, and structural information of the images, with values ranging from 0 to 1, where higher values indicate greater similarity. PSNR evaluates the similarity between images by computing the mean squared error between them. PSNR typically ranges from 0 to infinity and is measured in decibels (dB). Higher PSNR values indicate smaller differences between the images, reflecting higher similarity. In our ablation study, we utilize SSIM and PSNR to quantify the differences between the coarse or detail geometry shading sketches ($S^c_{t_j}$ or $S^d_{t_j}$) and the ground truth S_{t_j}, thereby quantitatively evaluating the impact of Φ_{detail} and $\mathcal{L}_{\text{sketch}}$ on visual quality.

4.3 Quantitative Comparison

Based on the Sketch-REALY benchmark, we comprehensively evaluated our methods with state-of-the-art approaches, including MGCNet [54], PRNet [20], HRN [37], Deep3D [17], 3DDFA-V2 [26], DECA [19], and DeepSketch2Face [28]. DeepSketch2Face [28] is a method tailored for sketch-to-3D-face reconstruction tasks, whereas [17, 19, 20, 26, 37, 54] are commonly used for reconstructing RGB face images. There are two ways to reconstruct 3D faces from sketches using these methods: firstly translating 2D sketches to face images [52] and subsequently reconstructing 3D faces or directly inputting sketches. To ensure fairness, we present the best results of these both ways for [17, 19, 20, 26, 37, 54]. The evaluation results on Sketch-REALY are shown in Tab.1. Tab.1 indicates that our method achieved the best results on both shading sketches (1.533mm in frontal-view and 1.506mm in side-view) and hard test cases with sparse line sketches (1.673mm in frontal-view and 1.690mm in side-view), surpassing the second-best method by a considerable margin, indicating that our method exhibits superior robustness to the type and pose of the input facial sketch.

4.4 Qualitative Comparison

Similar to Fig. 1, Fig. 6 further illustrates the visualization results of S2TD-Face. S2TD-Face is capable of reconstructing high-fidelity 3D faces consistent with the input sketch details from various styles. It can provide controllable textures based on text prompts, ranging from cartoon-style, sculptural style to realistic facial style. We also compared the reconstruction results of our method with those of DeepSketch2Face [28], Deep3D [17], and HRN [37], as shown in the Fig. 7. DeepSketch2Face [28] is limited to reconstructing 3D exaggerating faces from sketches with a frontal pose and cannot handle side views or adapt to various sketch styles. Deep3D [17] is only capable of reconstructing coarse geometry. While HRN [37] can capture high-frequency facial details, it may encounter failures in certain samples. The qualitative comparison indicates that S2TD-Face is capable of handling various styles and poses of

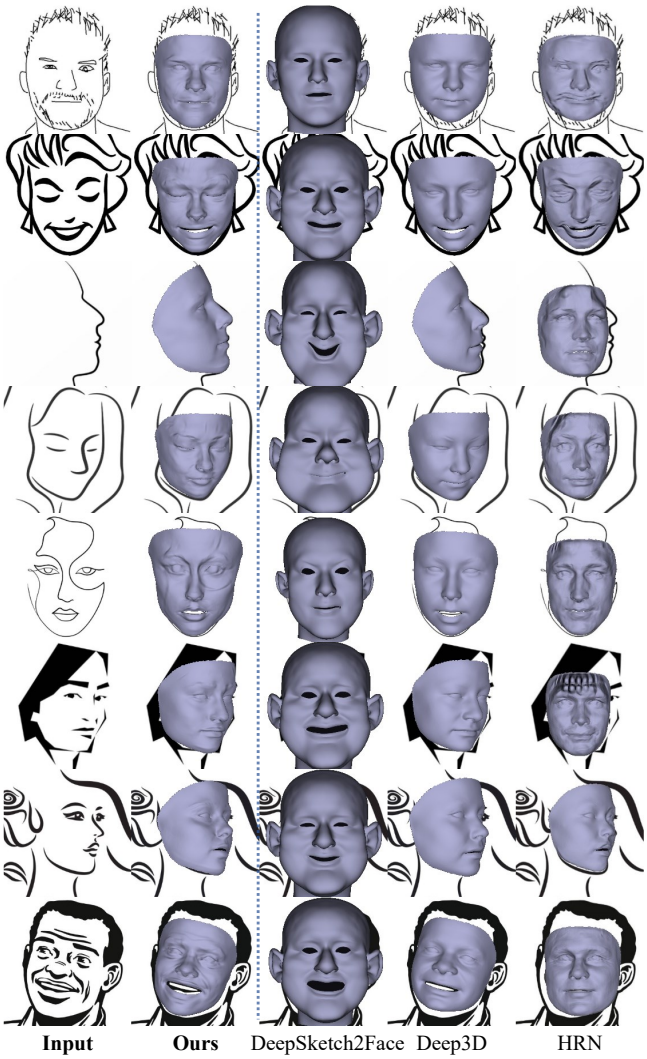

Figure 7: Qualitative comparison with the other methods. Our method (S2TD-Face) achieves the best results that consistent with the input sketch details.

facial sketches and achieves the best results consistent with the input sketch details. Note that these methods [17, 28, 37] all lack the ability to control the texture of the reconstructed 3D faces, while our S2TD-Face uniquely offers this capability.

4.5 Ablation Study

Impact of $\mathcal{L}_{\text{sketch}}$ on Geometry. We investigate the effect of sketch-to-geometry loss $\mathcal{L}_{\text{sketch}}$ for supervising geometry deformation. As shown in Tab. 1, based on our proposed geometry reconstruction framework and Sketch-REALY benchmark, we present results for both when the framework is applied independently (denoted as 'Ours (w/o $\mathcal{L}_{\text{sketch}}$)') and when combined with $\mathcal{L}_{\text{sketch}}$ (denoted as 'Ours'). The former indicates our geometry reconstruction framework performs superior to existing state-of-the-art methods across most cases. The latter further shows that incorporating $\mathcal{L}_{\text{sketch}}$ contributes to improved geometry deformation. The combination of $\mathcal{L}_{\text{sketch}}$ with our geometry reconstruction framework further refines the accuracy of the reconstructed geometry.

Table 2: Ablation study for the impact of $\mathcal{L}_{\text{sketch}}$ and Φ_{detail} on visual quality. Higher values indicate better results and the best is highlighted in bold.

Φ_{coarse}	$\mathcal{L}_{\text{sketch}}$	Φ_{detail}	SSIM ↑	PSNR ↑
✓	✗	✗	0.764	25.11
✓	✗	✓	0.776	25.22
✓	✓	✗	0.789	26.27
✓	✓	✓	**0.799**	**26.51**

Impact of $\mathcal{L}_{\text{sketch}}$ and Φ_{detail} on Visual Quality. We use SSIM and PSNR to investigate the impact of $\mathcal{L}_{\text{sketch}}$ and Φ_{detail} on visual quality. Utilizing rendering techniques [34, 51] and sketch extraction methods [7, 56, 57], we can acquire coarse or detailed geometry shading sketches ($S^c_{t_j}$ or $S^d_{t_j}$) for the predicted results. These sketches are subsequently compared with the ground truth S_{t_j} to compute the SSIM and PSNR scores. The test images are sourced from [9]. Quantitative results are shown in Tab.2. When neither $\mathcal{L}_{\text{sketch}}$ nor Φ_{detail} is involved, relying solely on Φ_{coarse} for reconstruction leads to poorer visual quality. Combining Φ_{coarse} with either $\mathcal{L}_{\text{sketch}}$ or Φ_{detail} individually results in improved visual quality, while employing $\mathcal{L}_{\text{sketch}}$ and Φ_{detail} together yields the best results. Note that comparing the second and third rows of Tab. 2, the combination of $\mathcal{L}_{\text{sketch}}$ with Φ_{coarse} even outperforms the combination of Φ_{detail} with Φ_{coarse}, further indicating the effectiveness of our proposed sketch-to-geometry loss $\mathcal{L}_{\text{sketch}}$ in faithfully capturing the geometric information of the input sketch.

4.6 Limitations

We summarize two limitations of our methods. Firstly, although Fig.1 and Fig.6 show that S2TD-Face can generate controllable textures based on text prompts, these textures are all obtained from existing facial images through UV-mapping and UV-texture-completion techniques. Low-frequency 3DMMs PCA albedo information is employed through the completion process, sometimes leading to noticeable visual differences at the fusion boundaries. Secondly, while our method can reconstruct high-fidelity geometry from face sketches of various styles, the geometry is derived from 3DMMs, resulting in the overall appearance still resembling real human faces when dealing with the animation styles.

5 CONCLUSIONS

This paper proposes a method tailored to the sketch-to-3D-face task, named S2TD-Face. S2TD-Face is capable of reconstructing high-fidelity topology-consistent detailed geometry from face sketches of diverse styles. It enables the controllable textures of 3D faces spanning cartoon, sculptural, and realistic facial styles based on text prompts. The contributions include an effective geometry reconstruction framework, a novel sketch-to-geometry loss for guiding geometry deformation, and a novel texture module for texture control based on text prompts. Extensive experiments show that the outstanding performance of our method surpasses existing state-of-the-art methods. The code will be publicly available.

REFERENCES

[1] Brian Amberg, Sami Romdhani, and Thomas Vetter. 2007. Optimal step nonrigid ICP algorithms for surface registration. In *2007 IEEE conference on computer vision and pattern recognition*. IEEE, 1–8.

[2] Haoran Bai, Di Kang, Haoxian Zhang, Jinshan Pan, and Linchao Bao. 2022. FFHQ-UV: Normalized Facial UV-Texture Dataset for 3D Face Reconstruction. *arXiv preprint arXiv:2211.13874* (2022).

[3] Hmrishav Bandyopadhyay, Subhadeep Koley, Ayan Das, Aneeshan Sain, Pinaki Nath Chowdhury, Tao Xiang, Ayan Kumar Bhunia, and Yi-Zhe Song. 2023. Doodle Your 3D: From Abstract Freehand Sketches to Precise 3D Shapes. *arXiv preprint arXiv:2312.04043* (2023).

[4] Volker Blanz and Thomas Vetter. 1999. A morphable model for the synthesis of 3D faces. In *Proceedings of the 26th annual conference on Computer graphics and interactive techniques*. 187–194.

[5] Volker Blanz and Thomas Vetter. 2003. Face recognition based on fitting a 3D morphable model. *IEEE Transactions on pattern analysis and machine intelligence* 25, 9 (2003), 1063–1074.

[6] Gary Bradski. 2000. The openCV library. *Dr. Dobb's Journal: Software Tools for the Professional Programmer* 25, 11 (2000), 120–123.

[7] Gary Bradski. 2000. The openCV library. *Dr. Dobb's Journal: Software Tools for the Professional Programmer* 25, 11 (2000), 120–123.

[8] Chen Cao, Yanlin Weng, Shun Zhou, Yiying Tong, and Kun Zhou. 2013. Facewarehouse: A 3d facial expression database for visual computing. *IEEE Transactions on Visualization and Computer Graphics* 20, 3 (2013), 413–425.

[9] Zenghao Chai, Haoxian Zhang, Jing Ren, Di Kang, Zhengzhuo Xu, Xuefei Zhe, Chun Yuan, and Linchao Bao. 2022. REALY: Rethinking the Evaluation of 3D Face Reconstruction. In *Computer Vision–ECCV 2022: 17th European Conference, Tel Aviv, Israel, October 23–27, 2022, Proceedings, Part VIII*. Springer, 74–92.

[10] Zenghao Chai, Tianke Zhang, Tianyu He, Xu Tan, Tadas Baltrusaitis, Hsiang-Tao Wu, Runnan Li, Sheng Zhao, Chun Yuan, and Jiang Bian. 2023. Hiface: High-fidelity 3d face reconstruction by learning static and dynamic details. In *Proceedings of the IEEE/CVF International Conference on Computer Vision*. 9087–9098.

[11] Dar-Yen Chen, Subhadeep Koley, Aneeshan Sain, Pinaki Nath Chowdhury, Tao Xiang, Ayan Kumar Bhunia, and Yi-Zhe Song. 2023. DemoCaricature: Democratising Caricature Generation with a Rough Sketch. (2023).

[12] Shu-Yu Chen, Feng-Lin Liu, Yu-Kun Lai, Paul L Rosin, Chunpeng Li, Hongbo Fu, and Lin Gao. 2021. Deepfaceediting: Deep face generation and editing with disentangled geometry and appearance control. *arXiv preprint arXiv:2105.08935* (2021).

[13] Shu-Yu Chen, Wanchao Su, Lin Gao, Shihong Xia, and Hongbo Fu. 2020. DeepFaceDrawing: Deep generation of face images from sketches. *ACM Transactions on Graphics (TOG)* 39, 4 (2020), 72–1.

[14] Wenzheng Chen, Huan Ling, Jun Gao, Edward Smith, Jaakko Lehtinen, Alec Jacobson, and Sanja Fidler. 2019. Learning to predict 3d objects with an interpolation-based differentiable renderer. *Advances in neural information processing systems* 32 (2019).

[15] Antonia Creswell, Tom White, Vincent Dumoulin, Kai Arulkumaran, Biswa Sengupta, and Anil A Bharath. 2018. Generative adversarial networks: An overview. *IEEE signal processing magazine* 35, 1 (2018), 53–65.

[16] Hang Dai, Nick Pears, William Smith, and Christian Duncan. 2020. Statistical modeling of craniofacial shape and texture. *International Journal of Computer Vision* 128 (2020), 547–571.

[17] Yu Deng, Jiaolong Yang, Sicheng Xu, Dong Chen, Yunde Jia, and Xin Tong. 2019. Accurate 3d face reconstruction with weakly-supervised learning: From single image to image set. In *Proceedings of the IEEE/CVF conference on computer vision and pattern recognition workshops*. 0–0.

[18] Abdallah Dib, Luiz Gustavo Hafemann, Emeline Got, Trevor Anderson, Amin Fadaeinejad, Rafael MO Cruz, and Marc-Andre Carbonneau. 2023. MoSAR: Monocular Semi-Supervised Model for Avatar Reconstruction using Differentiable Shading. *arXiv preprint arXiv:2312.13091* (2023).

[19] Yao Feng, Haiwen Feng, Michael J. Black, and Timo Bolkart. 2021. Learning an Animatable Detailed 3D Face Model from In-The-Wild Images. *ACM Transactions on Graphics, (Proc. SIGGRAPH)* 40, 8. https://doi.org/10.1145/3450626.3459936

[20] Yao Feng, Fan Wu, Xiaohu Shao, Yanfeng Wang, and Xi Zhou. 2018. Joint 3d face reconstruction and dense alignment with position map regression network. In *Proceedings of the European conference on computer vision (ECCV)*. 534–551.

[21] Clement Fuji Tsang, Maria Shugrina, Jean Francois Lafleche, Towaki Takikawa, Jiehan Wang, Charles Loop, Wenzheng Chen, Krishna Murthy Jatavallabhula, Edward Smith, Artem Rozantsev, Or Perel, Tianchang Shen, Jun Gao, Sanja Fidler, Gavriel State, Jason Gorski, Tommy Xiang, Jianing Li, Michael Li, and Rev Lebaredian. 2022. Kaolin: A Pytorch Library for Accelerating 3D Deep Learning Research. https://github.com/NVIDIAGameWorks/kaolin.

[22] Chenjian Gao, Qian Yu, Lu Sheng, Yi-Zhe Song, and Dong Xu. 2022. Sketchsampler: Sketch-based 3d reconstruction via view-dependent depth sampling. In *European Conference on Computer Vision*. Springer, 464–479.

[23] Lin Gao, Feng-Lin Liu, Shu-Yu Chen, Kaiwen Jiang, Chun-Peng Li, Yu-Kun Lai, and Hongbo Fu. 2023. SketchFaceNeRF: Sketch-Based Facial Generation and Editing in Neural Radiance Fields. *ACM Transactions on Graphics (Proceedings of ACM SIGGRAPH 2023)* 42, 4 (2023), 159:1–159:17.

[24] Baris Gecer, Stylianos Ploumpis, Irene Kotsia, and Stefanos Zafeiriou. 2019. Ganfit: Generative adversarial network fitting for high fidelity 3d face reconstruction. In *Proceedings of the IEEE/CVF conference on computer vision and pattern recognition*. 1155–1164.

[25] Benoit Guillard, Edoardo Remelli, Pierre Yvernay, and Pascal Fua. 2021. Sketch2mesh: Reconstructing and editing 3d shapes from sketches. In *Proceedings of the IEEE/CVF International Conference on Computer Vision*. 13023–13032.

[26] Jianzhu Guo, Xiangyu Zhu, Yang Yang, Fan Yang, Zhen Lei, and Stan Z Li. 2020. Towards fast, accurate and stable 3d dense face alignment. (2020), 152–168.

[27] Yudong Guo, Jianfei Cai, Boyi Jiang, Jianmin Zheng, et al. 2018. Cnn-based real-time dense face reconstruction with inverse-rendered photo-realistic face images. *IEEE transactions on pattern analysis and machine intelligence* 41, 6 (2018), 1294–1307.

[28] Xiaoguang Han, Chang Gao, and Yizhou Yu. 2017. DeepSketch2Face: a deep learning based sketching system for 3D face and caricature modeling. *ACM Transactions on graphics (TOG)* 36, 4 (2017), 1–12.

[29] Kaiming He, Xiangyu Zhang, Shaoqing Ren, and Jian Sun. 2016. Deep residual learning for image recognition. In *Proceedings of the IEEE conference on computer vision and pattern recognition*. 770–778.

[30] Phillip Isola, Jun-Yan Zhu, Tinghui Zhou, and Alexei A Efros. 2017. Image-to-image translation with conditional adversarial networks. In *Proceedings of the IEEE conference on computer vision and pattern recognition*. 1125–1134.

[31] Yueying Kao, Bowen Pan, Miao Xu, Jiangjing Lyu, Xiangyu Zhu, Yuanzhang Chang, Xiaobo Li, and Zhen Lei. 2023. Toward 3D Face Reconstruction in Perspective Projection: Estimating 6DoF Face Pose From Monocular Image. *IEEE Transactions on Image Processing* 32 (2023), 3080–3091. https://doi.org/10.1109/TIP.2023.3275535

[32] Tero Karras, Samuli Laine, and Timo Aila. 2019. A style-based generator architecture for generative adversarial networks. In *Proceedings of the IEEE/CVF conference on computer vision and pattern recognition*. 4401–4410.

[33] Diederik P Kingma and Jimmy Ba. 2014. Adam: A method for stochastic optimization. *arXiv preprint arXiv:1412.6980* (2014).

[34] Samuli Laine, Janne Hellsten, Tero Karras, Yeongho Seol, Jaakko Lehtinen, and Timo Aila. 2020. Modular Primitives for High-Performance Differentiable Rendering. *ACM Transactions on Graphics* 39, 6 (2020).

[35] Alexandros Lattas, Stylianos Moschoglou, Baris Gecer, Stylianos Ploumpis, Vasileios Triantafyllou, Abhijeet Ghosh, and Stefanos Zafeiriou. 2020. AvatarMe: Realistically Renderable 3D Facial Reconstruction" in-the-wild". In *Proceedings of the IEEE/CVF conference on computer vision and pattern recognition*. 760–769.

[36] Alexandros Lattas, Stylianos Moschoglou, Stylianos Ploumpis, Baris Gecer, Jiankang Deng, and Stefanos Zafeiriou. 2023. Fitme: Deep photorealistic 3d morphable model avatars. In *Proceedings of the IEEE/CVF Conference on Computer Vision and Pattern Recognition*. 8629–8640.

[37] Biwen Lei, Jianqiang Ren, Mengyang Feng, Miaomiao Cui, and Xuansong Xie. 2023. A Hierarchical Representation Network for Accurate and Detailed Face Reconstruction from In-The-Wild Images. In *Proceedings of the IEEE/CVF Conference on Computer Vision and Pattern Recognition*. 394–403.

[38] Shan Li and Weihong Deng. 2019. Blended Emotion in-the-Wild: Multi-label Facial Expression Recognition Using Crowdsourced Annotations and Deep Locality Feature Learning. *International Journal of Computer Vision* 127, 6-7 (2019), 884–906.

[39] Shan Li and Weihong Deng. 2019. Reliable Crowdsourcing and Deep Locality-Preserving Learning for Unconstrained Facial Expression Recognition. *IEEE Transactions on Image Processing* 28, 1 (2019), 356–370.

[40] Yuhang Li, Xuejin Chen, Binxin Yang, Zihan Chen, Zhihua Cheng, and Zheng-Jun Zha. 2020. Deepfacepencil: Creating face images from freehand sketches. In *Proceedings of the 28th ACM International Conference on Multimedia*. 991–999.

[41] Shichen Liu, Tianye Li, Weikai Chen, and Hao Li. 2019. Soft rasterizer: A differentiable renderer for image-based 3d reasoning. In *Proceedings of the IEEE/CVF International Conference on Computer Vision*. 7708–7717.

[42] Ziwei Liu, Ping Luo, Xiaogang Wang, and Xiaoou Tang. 2015. Deep Learning Face Attributes in the Wild. In *Proceedings of International Conference on Computer Vision (ICCV)*.

[43] Ling Luo, Pinaki Nath Chowdhury, Tao Xiang, Yi-Zhe Song, and Yulia Gryaditskaya. 2023. 3D VR Sketch Guided 3D Shape Prototyping and Exploration. In *Proceedings of the IEEE/CVF International Conference on Computer Vision*. 9267–9276.

[44] Tetiana Martyniuk, Orest Kupyn, Yana Kurlyak, Igor Krashenyi, Jiři Matas, and Viktoriia Sharmanska. 2022. DAD-3DHeads: A Large-scale Dense, Accurate and Diverse Dataset for 3D Head Alignment from a Single Image. In *Proc. IEEE Conf. on Computer Vision and Pattern Recognition (CVPR)*.

[45] Ben Mildenhall, Pratul P. Srinivasan, Matthew Tancik, Jonathan T. Barron, Ravi Ramamoorthi, and Ren Ng. 2020. NeRF: Representing Scenes as Neural Radiance Fields for View Synthesis. In *ECCV*.

[46] Jeong Joon Park, Peter Florence, Julian Straub, Richard Newcombe, and Steven Lovegrove. 2019. Deepsdf: Learning continuous signed distance functions for shape representation. In *Proceedings of the IEEE/CVF conference on computer vision and pattern recognition*. 165–174.

[47] Adam Paszke, Sam Gross, Francisco Massa, Adam Lerer, James Bradbury, Gregory Chanan, Trevor Killeen, Zeming Lin, Natalia Gimelshein, Luca Antiga, et al. 2019. Pytorch: An imperative style, high-performance deep learning library. *Advances in neural information processing systems* 32 (2019).

[48] Pascal Paysan, Reinhard Knothe, Brian Amberg, Sami Romdhani, and Thomas Vetter. 2009. A 3D face model for pose and illumination invariant face recognition. In *2009 sixth IEEE international conference on advanced video and signal based surveillance*. Ieee, 296–301.

[49] Alec Radford, Jong Wook Kim, Chris Hallacy, Aditya Ramesh, Gabriel Goh, Sandhini Agarwal, Girish Sastry, Amanda Askell, Pamela Mishkin, Jack Clark, et al. 2021. Learning transferable visual models from natural language supervision. In *International conference on machine learning*. PMLR, 8748–8763.

[50] Ravi Ramamoorthi and Pat Hanrahan. 2001. An efficient representation for irradiance environment maps. In *Proceedings of the 28th annual conference on Computer graphics and interactive techniques*. 497–500.

[51] Nikhila Ravi, Jeremy Reizenstein, David Novotny, Taylor Gordon, Wan-Yen Lo, Justin Johnson, and Georgia Gkioxari. 2020. Accelerating 3D Deep Learning with PyTorch3D. *arXiv:2007.08501* (2020).

[52] Elad Richardson, Yuval Alaluf, Or Patashnik, Yotam Nitzan, Yaniv Azar, Stav Shapiro, and Daniel Cohen-Or. 2021. Encoding in style: a stylegan encoder for image-to-image translation. In *Proceedings of the IEEE/CVF conference on computer vision and pattern recognition*. 2287–2296.

[53] Christos Sagonas, Georgios Tzimiropoulos, Stefanos Zafeiriou, and Maja Pantic. 2013. 300 faces in-the-wild challenge: The first facial landmark localization challenge. In *Proceedings of the IEEE international conference on computer vision workshops*. 397–403.

[54] Jiaxiang Shang, Tianwei Shen, Shiwei Li, Lei Zhou, Mingmin Zhen, Tian Fang, and Long Quan. 2020. Self-supervised monocular 3d face reconstruction by occlusion-aware multi-view geometry consistency. In *Computer Vision–ECCV 2020: 16th European Conference, Glasgow, UK, August 23–28, 2020, Proceedings, Part XV*. Springer, 53–70.

[55] Dave Shreiner, Bill The Khronos OpenGL ARB Working Group, et al. 2009. *OpenGL programming guide: the official guide to learning OpenGL, versions 3.0 and 3.1*. Pearson Education.

[56] Edgar Simo-Serra, Satoshi Iizuka, and Hiroshi Ishikawa. 2018. Mastering sketching: adversarial augmentation for structured prediction. *ACM Transactions on Graphics (TOG)* 37, 1 (2018), 1–13.

[57] Edgar Simo-Serra, Satoshi Iizuka, Kazuma Sasaki, and Hiroshi Ishikawa. 2016. Learning to simplify: fully convolutional networks for rough sketch cleanup. *ACM Transactions on Graphics (TOG)* 35, 4 (2016), 1–11.

[58] Zhou Wang, Alan C Bovik, Hamid R Sheikh, and Eero P Simoncelli. 2004. Image quality assessment: from error visibility to structural similarity. *IEEE transactions on image processing* 13, 4 (2004), 600–612.

[59] Zidu Wang, Xiangyu Zhu, Tianshuo Zhang, Baiqin Wang, and Zhen Lei. 2023. 3D Face Reconstruction with the Geometric Guidance of Facial Part Segmentation. *arXiv preprint arXiv:2312.00311* (2023).

[60] Peng Xu, Timothy M Hospedales, Qiyue Yin, Yi-Zhe Song, Tao Xiang, and Liang Wang. 2022. Deep learning for free-hand sketch: A survey. *IEEE transactions on pattern analysis and machine intelligence* 45, 1 (2022), 285–312.

[61] Li Yang, Jing Wu, Jing Huo, Yu-Kun Lai, and Yang Gao. 2021. Learning 3D face reconstruction from a single sketch. *Graphical Models* 115 (2021), 101102.

[62] Song-Hai Zhang, Yuan-Chen Guo, and Qing-Wen Gu. 2021. Sketch2model: View-aware 3d modeling from single free-hand sketches. In *Proceedings of the IEEE/CVF Conference on Computer Vision and Pattern Recognition*. 6012–6021.

[63] Qi Zheng, Jiankang Deng, Zheng Zhu, Ying Li, and Stefanos Zafeiriou. 2022. Decoupled Multi-task Learning with Cyclical Self-Regulation for Face Parsing. In *Computer Vision and Pattern Recognition*.

[64] Xin-Yang Zheng, Hao Pan, Peng-Shuai Wang, Xin Tong, Yang Liu, and Heung-Yeung Shum. 2023. Locally attentional sdf diffusion for controllable 3d shape generation. *ACM Transactions on Graphics (TOG)* 42, 4 (2023), 1–13.

[65] Xiangyu Zhu, Zhen Lei, Junjie Yan, Dong Yi, and Stan Z Li. 2015. High-fidelity pose and expression normalization for face recognition in the wild. In *Proceedings of the IEEE conference on computer vision and pattern recognition*. 787–796.

[66] Xiangyu Zhu, Xiaoming Liu, Zhen Lei, and Stan Z Li. 2017. Face alignment in full pose range: A 3d total solution. *IEEE transactions on pattern analysis and machine intelligence* 41, 1 (2017), 78–92.

[67] Xiangyu Zhu, Chang Yu, Di Huang, Zhen Lei, Hao Wang, and Stan Z Li. 2022. Beyond 3DMM: Learning to Capture High-fidelity 3D Face Shape. *IEEE Transactions on Pattern Analysis and Machine Intelligence* (2022).